chemosensors

MDPI

Article

Low-Cost Carbon Paste Cu(II)-Exchanged Zeolite Amperometric Sensor for Hydrogen Peroxide Detection

Delia Gligor [1], Sanda Andrada Maicaneanu [2] and Codruta Varodi [3,*]

[1] Department of Environmental Analysis and Engineering, Babes-Bolyai University, 30 Fantanele St., 400294 Cluj-Napoca, Romania; delia.gligor@ubbcluj.ro
[2] Madia Department of Chemistry, Biochemistry, Physics and Engineering, Indiana University of Pennsylvania, 421 North Walk, Indiana, PA 15705, USA; sanda.maicaneanu@iup.edu
[3] National Institute for Research and Development of Isotopic and Molecular Technologies, 67-103 Donat St., 400293 Cluj-Napoca, Romania
* Correspondence: codruta.varodi@itim-cj.ro

Abstract: The aim of this work was to explore the possibility of using a Cu-exchanged zeolitic volcanic tuff (which is natural and easy to prepare and apply) for the preparation of a new low-cost carbon paste amperometric sensor for H_2O_2 detection. The properties of the zeolitic volcanic tuff were determined using chemical analysis, energy-dispersive X-ray spectroscopy, the specific surface area, electron microscopy, X-ray diffraction spectroscopy, and Fourier-transform infrared spectroscopy. The sensor was successfully built and operates at pH 7, at an applied potential of −150 mV Ag/AgCl/KCl_{sat}, presenting a sensitivity of 0.87 mA M^{-1}, a detection limit of 10 μM and a linear domain up to 30 mM H_2O_2. These good electroanalytic parameters for H_2O_2 detection (a low detection limit and high sensitivity) support the possibility of using these sensors for the detection of many analytes in environmental, food and medical applications.

Keywords: carbon paste electrodes; zeolite; amperometric sensor; hydrogen peroxide

Citation: Gligor, D.; Maicaneanu, S.A.; Varodi, C. Low-Cost Carbon Paste Cu(II)-Exchanged Zeolite Amperometric Sensor for Hydrogen Peroxide Detection. *Chemosensors* **2024**, *12*, 23. https://doi.org/10.3390/chemosensors12020023

Academic Editors: Joana Rodrigues and Nuno Santos

Received: 27 December 2023
Revised: 30 January 2024
Accepted: 31 January 2024
Published: 4 February 2024

1. Introduction

Zeolites are widely used in the environmental remediation of soil or water to immobilize or remove toxic materials by cation exchange, e.g., Cu [1], due to their channel network and exchangeable cations. They have specific properties: their adsorption–desorption capacity, ion exchange capacity and catalytic properties [2]. Their ionic exchange capacity allows for the modification of natural or synthetic zeolites with metal ions. Such modification of zeolites opens up new ways in which they can be used.

Copper-modified zeolites have many applications: some modified electrodes prepared using an aqueous ion-exchange method on synthetic zeolites have been tested for their electrochemical stability [3]; other modified electrodes have been used as electrochemical sensors for the determination of dopamine, ascorbic acid and non-electroactive cations [4–8].

Hydrogen peroxide (H_2O_2) is a bleaching agent used in the textile and paper industries and shows oxidizing properties [9]. It is used as a disinfectant and antiseptic and as an oxidizer for solid rocket propulsion [10], and is produced naturally in organisms as a by-product of metabolism, regulating numerous states of oxidative stress [11,12].

Additionally, H_2O_2 has an important role in natural oxidation processes because it is found in air, water and solid foods. It is an analyte used in food [13], agricultural [14], pharmaceutical [15], clinical [16], industrial and environmental analyses [17,18]. Techniques for detecting H_2O_2 include colorimetry [19,20], spectrometry [21], chemiluminescence [22,23], titrimetry [24], spectrophotometry [25], fluorimetry [26–32], the use of fiber-optic devices [33] and chromatography [34], but most of these are time-consuming, use expensive reagents and suffer with interference from various species. As such, the use

of electrochemical methods such as voltammetry and amperometry presents advantages, such as low detection limits and a rapid response time [35–48].

Taking into account all these considerations, the novelty of this work was to prepare a new, low-cost carbon paste amperometric sensor for H_2O_2 detection based on Cu-exchanged zeolitic volcanic tuff. The obtained amperometric sensor is low cost due to the natural materials used to create it (natural zeolite), and it is easy to prepare and apply. The advantages of this natural zeolite are its low energy consumption and the lack of pollutants created throughout its entire life cycle, as well as the fact that it is found in high quantities in the environment. Additionally, the chemical composition of the natural zeolite was the same for many samples that were used to prepare the H_2O_2 amperometric sensors, due to the high quality (homogeneity and zeolite content) of the deposit where the samples were collected from.

The modified electrodes show good electroanalytic parameters for H_2O_2 detection (a low detection limit and high sensitivity), which supports the possibility of using them to detect many analytes in environmental, food and medical applications.

The modified zeolite was characterized using different methods (chemical analysis, energy-dispersive X-ray spectroscopy, electron microscopy, X-ray diffraction spectroscopy and Fourier-transform infrared spectroscopy). The copper-exchanged zeolite-modified electrode was characterized using cyclic voltammetry and amperometry techniques.

2. Materials and Methods

2.1. Materials

Hydrogen peroxide, NaCl, $CuSO_4 \cdot 5H_2O$ and 25% ammonium solution were acquired from Reactivul, Bucharest, Romania, and graphite powder and paraffin oil were purchased from Fluka (Buchs, Switzerland).

For the preparation of phosphate-buffered solution, we employed $K_2HPO_4 \cdot 2H_2O$ and $KH_2PO_4 \cdot H_2O$ from Merck (Darmstadt, Germany).

2.1.1. Preparation of the Modified Zeolite

The zeolitic tuff sample was collected from a natural outcrop in Macicas (Cluj County, Romania). To prepare the electrode material, the zeolitic tuff sample was ground to 0.2–0.4 mm (based on a previous test which showed that this fraction is the best for retaining metal ions in fixed-bed column experiments) via grinding and size separation, then washed with distilled water and dried at 105 °C. This physical treatment was followed by an alkaline treatment (NaCl 1 M), as described in a previous work [49].

Modification of the zeolitic tuff sample was realized by contact with a copper synthetic aqueous solution in dynamic conditions. The ionic exchange process took place, as shown in Equation (1), when copper solution (0.25–16.6 g Cu^{2+}/L prepared from analytical-purity $CuSO_4 \cdot 5H_2O$) was passed through a column containing 2.5 g of zeolitic volcanic tuff (flooded, d_i = 15 mm) at a flow rate of 0.07 mL/s, as previously described [2]. The experiments were realized at room temperature (22 ± 2 °C), without any pH adjustments, until exhaustion of the zeolite volcanic tuff sample took place. Samples obtained in this way were further subjected to drying at 105 °C for 6 h and calcination at 400 °C (in air) for 4 h. The amount of copper incorporated into the zeolite sample was determined using the initial and final concentrations of copper ions in solution, determined by spectrophotometric measurements (Jenway 6305 spectrophotometer, Vernon Hills, Illinois, USA, 25% ammonium solution, λ_{max} = 440 nm):

$$2Z - Na + Cu^{2+} \leftrightarrows Z_2 - Cu + 2Na^+ \quad (1)$$

Cu–Z-modified zeolitic volcanic tuff was further used to prepare the modified carbon-paste electrodes.

2.1.2. Electrode Preparation

The zeolites were mixed with graphite (2:1, w/w) and paraffin oil to obtain carbon paste electrodes modified with zeolite (Z-CPEs) and carbon paste electrodes modified with Cu-enriched zeolite (Cu–Z-CPEs).

All the compounds were manually mixed in an agate mortar and pestle for 10 min and the resulting samples were introduced into a Teflon tube equipped with an electrical copper wire contact for external connection to the potentiostat/galvanostat. Finally, the electrode's surface preparation included a polishing step, carried out multiple times using regular paper.

2.2. Methods

2.2.1. Physical and Chemical Characterization

The zeolitic volcanic tuff, in natural (Z) and modified (Cu–Z) forms, was characterized using chemical analysis, energy dispersive X-ray spectroscopy (EDS), specific surface area (BET), scanning and transmission electron microscopy (SEM, TEM), X-ray diffraction spectroscopy (XRD) and Fourier-transform infrared spectroscopy (FTIR).

Chemical analysis of the bulk sample was realized using specific analytical methods for silicate materials. Oxford Instruments EDS–Inca apparatus (Abingdon, United Kingdom) was used for surface elemental analysis (EDS).

Measurement of the BET surface area (S_{BET}) and pore size distribution was performed using approximately 0.2 g of sample degassed in a vacuum at 106 °C for 20 h to remove all the adsorbed species. A Sorptomatic 1990 (Thermo Electron Corporation, Waltham, MA, USA) was used to record the nitrogen adsorption and desorption isotherms.

Powder X-ray diffraction was performed using a Siemens Bruker unit with a Cu Kα anticathode. Diffraction patterns were obtained in the $5^\circ \div 50^\circ$ 2θ range and the following analytical conditions: 20 kV, 40 mA and a step of 2 degrees. The mineral composition was determined using a semi-quantitative X-ray diffraction method.

SEM images were obtained from samples deposited on double adhesive carbon discs, covered with 10 nm Au in an Agar Automated Sputter Coater and examined using a Jeol JSM5510Lvscanning electron microscope (Peabody, MA, USA). TEM images were obtained from samples suspended in distilled water (ultrasonic bath), deposited on a 300-mesh electrolytic grid, covered with carbon film (freshly deposited in vacuum) and examined using a Jeol JEM1010 transmission electron microscope (Peabody, MA, USA)).

A Jasco 615 spectrophotometer (Tokyo, Japan) was used to collect the FTIR spectra in the 400–4000 cm^{-1} range, with a resolution of 2 cm^{-1}, on KBr pellets (2 mg sample in 200 mg KBr).

2.2.2. Electrochemical Measurements

A PC-controlled electrochemical analyzer (Autolab-PGSTAT 10, EcoChemie, Utrecht, The Netherlands) managed by GPES 4.8 (General Purpose Electrochemical System software package) was used for cyclic voltammetry and amperometry measurements, while a EG&G rotator (Radiometer) was used to modulate the stirring rate of the working electrode. The carbon paste electrode (CPE) was the working electrode, the Ag/AgCl (3.0 mol L^{-1} KCl) was used as the reference electrode and a platinum electrode was used as a counter electrode.

A pH-meter (HI255, Hanna Instruments, Cluj-Napoca, Romania) equipped with a HI1131B glass electrode was used to adjust the pH during the addition of the phosphate buffer solutions.

3. Results and Discussion

3.1. Physical and Chemical Characterization of Natural and Modified Zeolite Samples

The zeolitic tuff samples were collected from an outcrop in Macicas (Cluj County, Romania). This deposit belongs to the Dej Tuff Level and it is of lower Badenian age. From a structural point of view, volcanic tuffs from Macicas are massive cinerites represented

by vitric-crystal and vitric tuffs. The main petrographical component is represented by white-greyish or white-greenish volcanic tuff that may be interlayered with marls and clays. Depending on the level, volcanic tuff varies from fine microporous to compact macroporous [2].

The bulk chemical composition of the natural zeolitic tuff sample was determined to be as follows, in mass %: SiO_2 63.91, Al_2O_3 14.45, Fe_2O_3 1.74, CaO 5.34, MgO 0.30, Na_2O 1.02, K_2O 0.86, TiO_2 0.38 and loss of ignition at 1000 °C (L.O.I.) 12. The value of the L.O.I. indicates that secondary and hydrated materials (zeolite and clay minerals) are present in high amounts. The tuff samples collected from the studied area are remarkably homogeneous in their mineralogical and chemical composition [49,50].

Figure 1A, B presents the SEM–EDS spectra and atomic weight composition of the Z (A) and Cu–Z (B) samples. The EDS spectra for the natural sample indicates the following elemental composition: Si, Al, Na, K, Ca, Mg and O (Figure 1A). For the Cu–Z-modified sample, copper was identified alongside the main elements; Figure 1B. Several surface regions of the Cu–Z and Cu–Z-CPE samples were analyzed; copper amounts of between 1.3 and 6.6% (average 3.95%) were determined. A high quantity of carbon from graphite, up to 74.3%, was identified when the electrode material was subjected to EDS analysis.

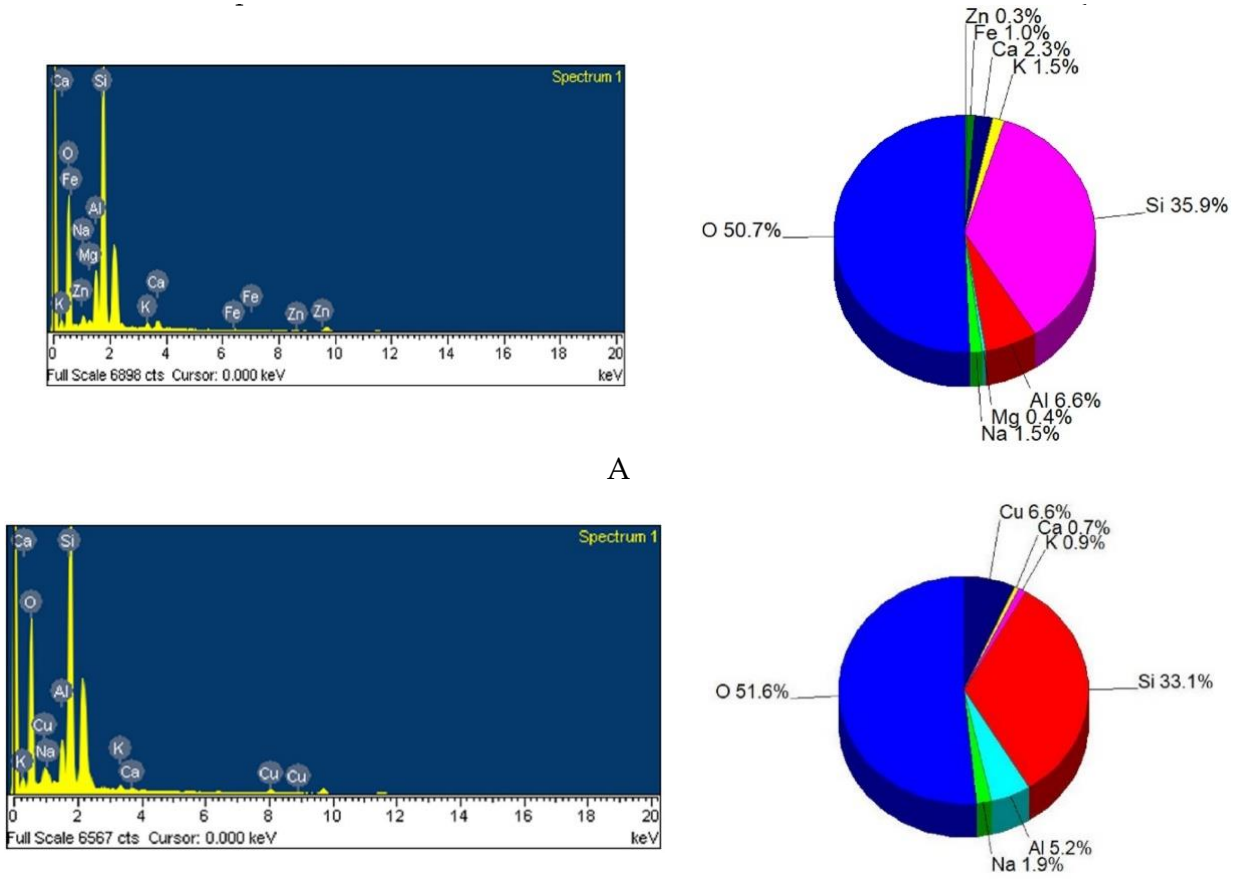

Figure 1. SEM–EDS spectra and atomic weight composition of the Z (**A**) and Cu–Z (**B**) samples.

According to N_2 adsorption and desorption isotherm investigations, the BET specific surface area of the unmodified zeolitic volcanic tuff sample had an average value of 35.7 m^2/g, while after modification, a small decrease was observed—most probably due to the thermal treatment applied (down to 30 m^2/g). The adsorption–desorption isotherm, shown in Figure 2A, is of type II with a H3 type loop, typical of slit-shaped pores [51]. The pore size distribution, shown in Figure 2B, indicates that the considered samples had a

multimodal distribution of mesopores in the small-size region (3–13 nm). For the modified sample, a change in the pore size distribution was observed, which can be attributed to the alteration of the pore size during the thermal treatment (pore volumes corresponding to small pores decreased, while new nodal positions appeared at higher pore diameters).

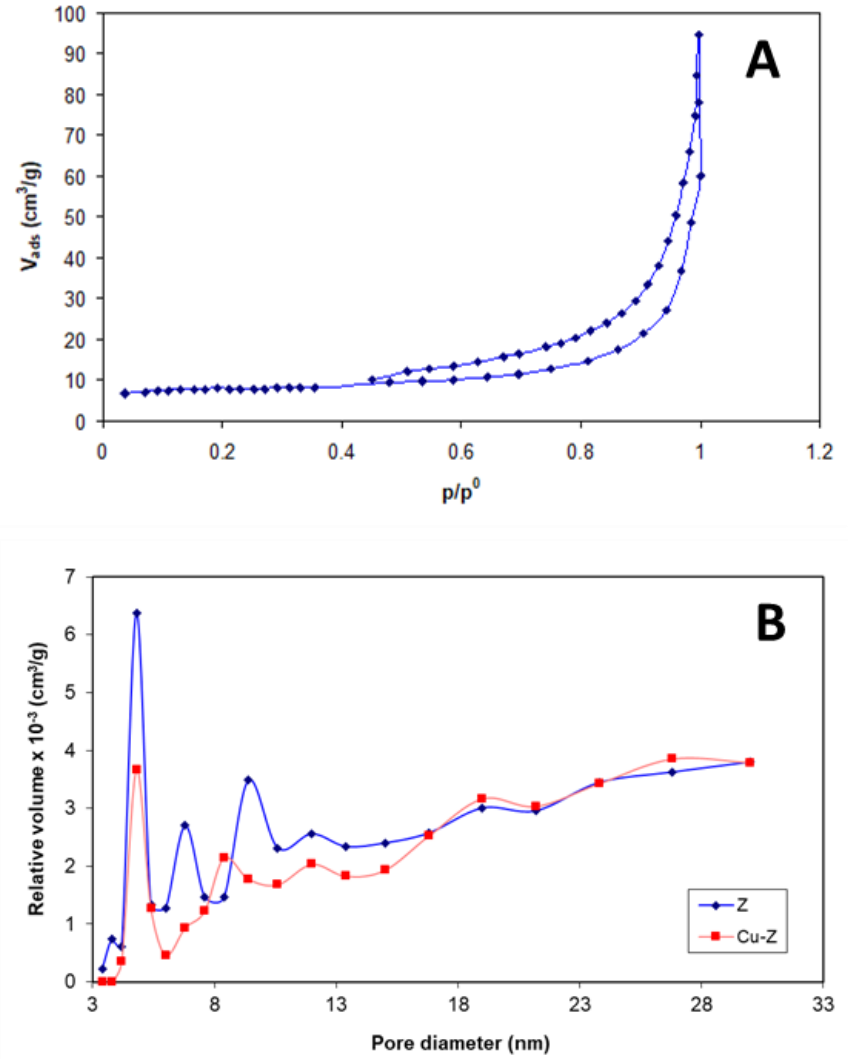

Figure 2. N_2 adsorption–desorption isotherm for an unmodified sample, Z (**A**) and BJH pore size distribution (**B**) for an unmodified (Z) and Cu-modified sample (Cu–Z).

XRD powder diffractograms indicated that clinoptilolite was present in substantial amounts and was the main zeolite species present. Based on a semi-quantitative estimation, the zeolite—clinoptilolite—represented 70–80% of the crystallized fraction of the tuff. Quartz, plagioclase, biotite and montmorillonite were identified as accompanying minerals [2,49,50].

SEM and TEM images of the unmodified zeolitic volcanic tuff sample show that the zeolite was present as tabular clinoptilolite crystals, shown in Figure 3, which varied in size from 2 to 10 µm. Larger crystals were usually found in the pores of the bulk rock.

FTIR measurements were also used to characterize the samples of zeolitic volcanic tuff and confirm the presence of clinoptilolite. Spectra of the natural sample (Figure 4) confirmed the presence of specific zeolite peaks, identified in Table 1, in accordance with the literature data [2,52–55]. For the Cu–Z sample, some minor modifications—specifically, peak shifts (Figure 4)—were observed. This can be attributed to the partial destruction of the zeolite's three-dimensional structure during the calcination process [2].

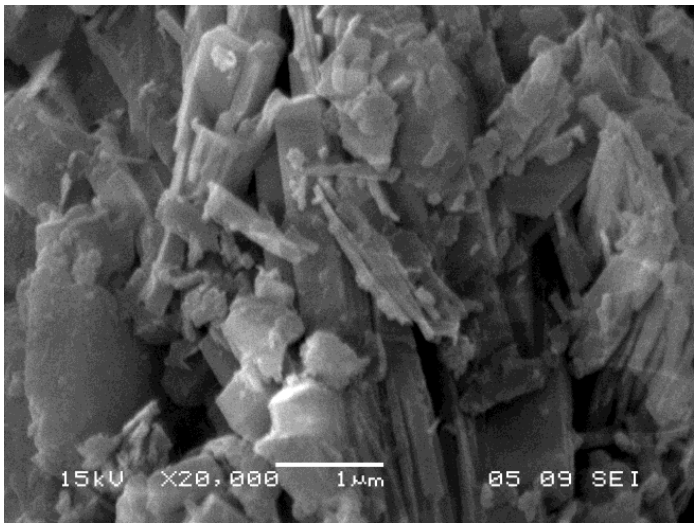

(**A**)

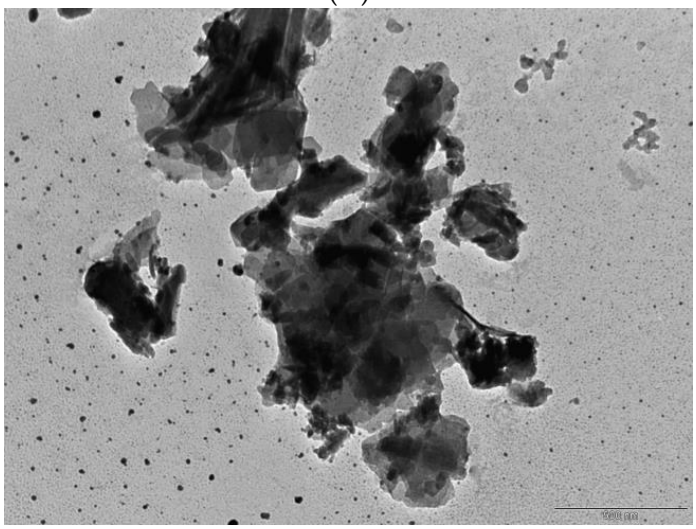

(**B**)

Figure 3. SEM (**A**) of TEM (**B**, scale 500 nm) images of the unmodified zeolitic volcanic tuff.

Table 1. The infrared bands of the Z and Cu–Z samples.

	Sample			Shift [b]	IR Signal Attribution
	Z	Cu–Z	Z [a]		
Wavenumber (cm^{-1})	3620	3620	3610	-	O–H bond stretching
	3446	3446	-	-	O–H bond stretching
	1637	1637	1635	-	H–O–H angular deformation
	1209	shoulder	1210	↓↓	(Si, Al)–O asymmetric internal stretching
	1055	1074	1070	↑	(Si, Al)–O asymmetric external stretching
	796	788	790	↓	(Si, Al)–O external symmetric stretching
	733	726	740	↓	(Si, Al)–O external symmetric stretching
	669	674	670	↑	(Si, Al)–O external symmetric stretching
	606	607	602	↑	ring-coupled (Si, Al)–O external vibration
	467	459	465	↓	O–(Si, Al)–O angular deformation

[a] literature data [2,53–55]. [b] IR band shift—↑ towards higher values, ↓ towards smaller values—Z vs. Cu–Z.

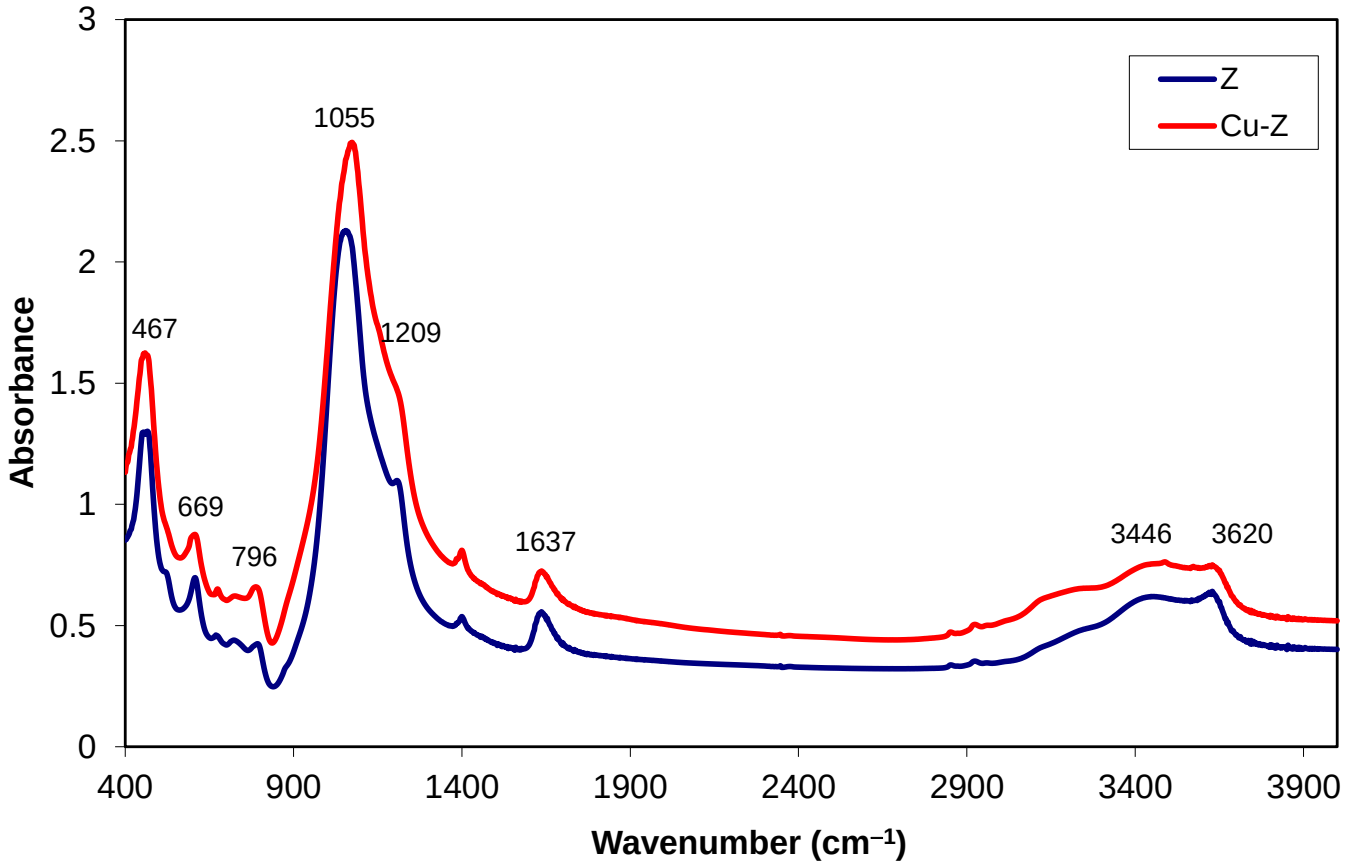

Figure 4. FTIR spectra of the unmodified Z and copper modified Cu–Z zeolitic volcanic.

The breakthrough curve (time vs. concentration evolution) and cation exchange capacity during the ionic exchange process and modification of the zeolitic tuff sample, (up to 225 min, 900 mL copper solution) are presented in Figure 5. The cation exchange capacity ("practical capacity" or "operating capacity" obtained under working conditions) [56,57], in mg/g, was calculated by taking into consideration the initial concentration times *t* concentration and the zeolitic volcanic tuff mass placed in the column. Following the ionic exchange process evolution, shown in Figure 5A, it was observed that as the copper ion initial concentration decreased, the breakthrough curve slope angle was smaller, indicating that the ionic exchange reaction rate decreased and therefore that the ionic exchange capacity had a smaller value; Figure 5B. Additionally, when a concentrated copper ion solution made contact with the zeolitic volcanic tuff, the ionic exchange capacity increased abruptly—up to 262.6 mg/g—showing a high capacity of the sample to retain metal ions when mass transfer conditions are improved. The maximum calculated cation exchange capacity values are presented in Figure 6.

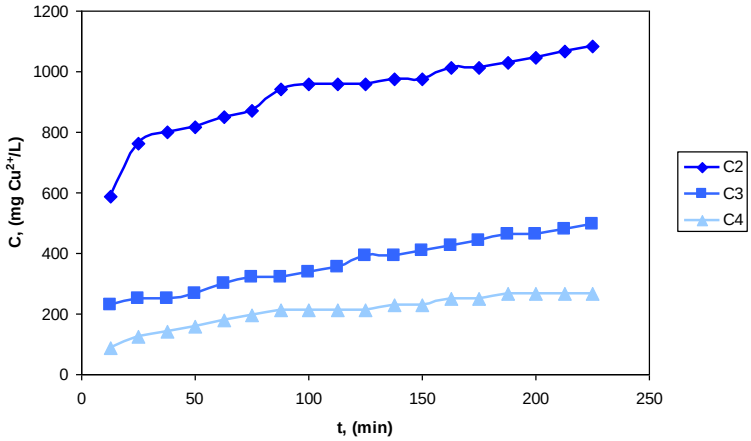

(**A**)

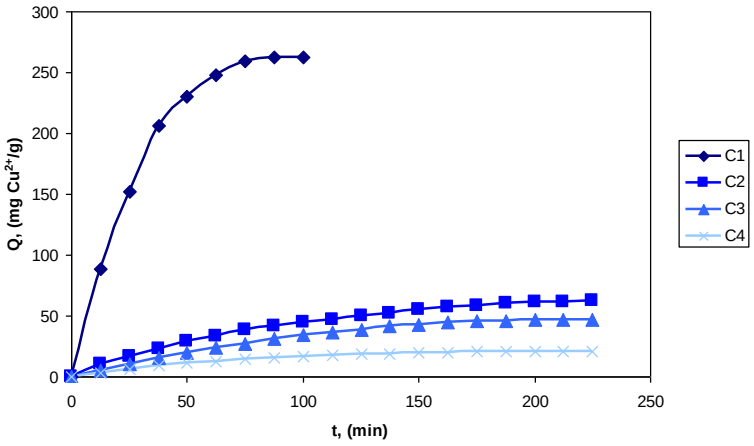

(**B**)

Figure 5. (**A**) Evolution over time of copper exchange capacity values (corresponding to the breakthrough curve) and (**B**) cation exchange capacity during the ionic exchange process; C1 = 16.6 g Cu^{2+}/L, C2 = 1.10 g Cu^{2+}/L, C3 = 0.50 g Cu^{2+}/L, C4 = 0.25 g Cu^{2+}/L, grain size 0.2–0.4 mm, flow rate 0.055 mL/min.

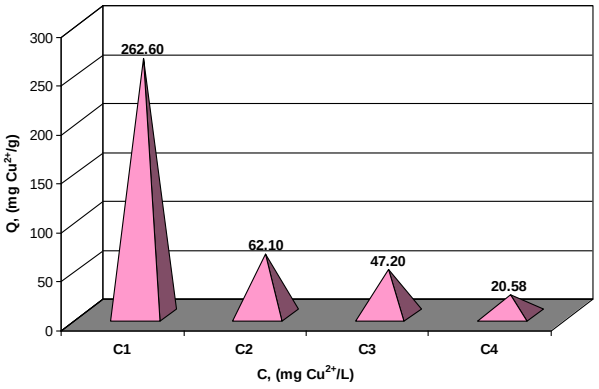

Figure 6. Maximum copper exchange capacity values on the zeolitic volcanic tuff sample; C1 = 16.5 g Cu^{2+}/L, C2 = 1.10 g Cu^{2+}/L, C3 = 0.50 g Cu^{2+}/L, C4 = 0.25 g Cu^{2+}/L.

3.2. Electrochemical and H_2O_2 Electrocatalytic Measurements

The electrochemical characterization of the newly obtained modified electrodes was realized in different experimental conditions to determine the electrochemical parame-

ters and to study the influence of the supporting electrolyte pH and scan rate on the voltammetric response.

The obtained electrodes were first electrochemically tested in a phosphate buffer solution to observe their voltammetric response. As can be seen in Figure 7A, in phosphate buffer solution as the supporting electrolyte, at 7 pH and a scan rate of 10 mV s^{-1}, the copper-enriched zeolite-modified electrodes (Cu–Z-CPEs) showed better voltammetric signals than the carbon paste electrodes modified with zeolites (Z-CPEs) and unmodified carbon paste electrodes (CPEs). The redox peak pair can be atributed to the oxidation and reduction of the copper available in the modified natural zeolite. The electrochemical parameters for Cu–Z-CPEs are as follows: the anodic peak potential E_{pa} = −235 mV vs. $Ag/AgCl/KCl_{sat}$; the cathodic peak potential E_{pc} = −5 mV vs. $Ag/AgCl/KCl_{sat}$; the formal standard potential (calculated as average of anodic and cathodic peak potential) $E^{0'}$ = −120 mV vs. $Ag/AgCl/KCl_{sat}$; the I_{pa}/I_{pc} ratio = 3.12; surface coverage $\Gamma = 2.2 \cdot 10^{-7}$ mol cm^{-2}, according to [58].

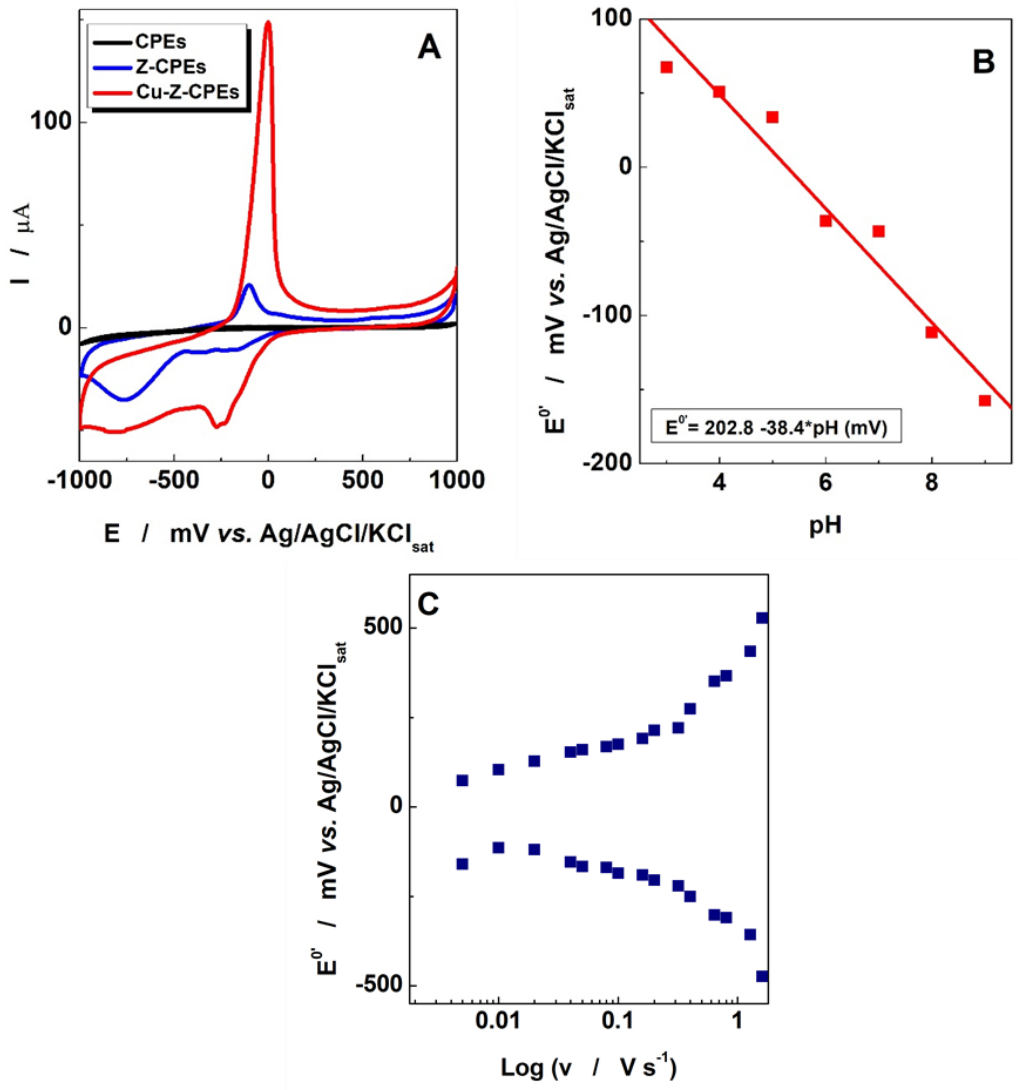

Figure 7. Cyclic voltammograms corresponding to the obtained modified electrodes (**A**); pH dependence of formal standard potential (**B**) and experimental dependence of ($E_p - E^{0'}$) on the logarithm of the scan rate (**C**) corresponding to Cu–Z–CPEs. Experimental conditions: starting potential,—1000 mV vs. $Ag/AgCl/KCl_{sat}$; scan rate, 10 mV s^{--1} (**A**); 50 mV s^{--1} (**B**); supporting electrolyte, 0.1 M phosphate buffer solution, pH 7 (**A**,**C**).

All further experiments were realized with phosphate buffer as the supporting electrolyte, with different pH values. As was expected, the $E^{0'}$ values were dependent on the supporting electrolyte pH in the case of the obtained carbon paste electrodes. The slope of the linear regression corresponding to the $E^{0'}$ vs. pH dependence (Figure 7B) was close to 0.059 V/ΔpH, which indicates that a transfer of $2e^-/2H^+$ was involved in the redox process and that the transfer electrons varied with the pH. This pH influence on the voltammetric response of the newly obtained electrodes will be useful for further investigations on H_2O_2 electrocatalytic activity.

Cyclic voltammetric measurements were recorded at increased electrode potential scan rates (Figure S1) to determine the kinetic parameters of the copper electron transfer, using the method proposed by Laviron [59]. From the influence of the formal standard potential $E^{0'}$ on the log of the scan rate (Figure 7C), the rate constant of the heterogeneous electron transfer k_s of 1.74 s^{-1} and the transfer coeficient α of 0.74 were evaluated for the obtained modified electrodes (Cu–Z-CPEs). This value of the heterogeneous electron transfer rate constant proves that copper can be used as an efficient mediator for electron transfer.

Additionally, the scan rate influence on the peak current was studied by recording the voltammograms at different potential scan rates. The cyclic voltammograms measurements performed at different potential scan rates, between 0.01 and 1.8 V s^{-1}, and showed a linear dependence of anodic and cathodic peak current intensity (I_{pa} and I_{pc}) on the potential scan rate (v). At different supporting electrolyte pHs, the slopes of the log I_p vs. log v dependence were close to 0.5, confirming the existance of a diffusion control (Table 2).

Table 2. Parameters of the log linear regression corresponding to the peak current dependence on the potential scan rate for Cu–Z-CPEs. Experimental conditions as in Figure 7.

pH	Slope		R/No. of Exp. Points	
	Oxidation	Reduction	Oxidation	Reduction
3	0.56 ± 0.02	0.62 ± 0.03	0.995/9	0.992/9
5	0.34 ± 0.01	0.51 ± 0.03	0.996/13	0.985/13
7	0.41 ± 0.02	0.60 ± 0.02	0.990/10	0.994/14
9	0.40 ± 0.03	0.57 ± 0.02	0.970/12	0.995/15

The electrocatalytic characterization of H_2O_2 reduction was first studied using cyclic voltammetric measurements, to determine the electrocatalytic efficiency.

The cyclic voltammograms recorded in phosphate buffer solution at pH 7 and a scan rate of 10 mV s^{-1} for the obtained carbon paste electrodes (Cu-Z-CPEs), in the absence and in the presence of H_2O_2 solution at two concentrations (1 mM and 5 mM; Figure 8), proved the presence of good electrocatalytic activity towards H_2O_2 reduction, as characterized by: (i) decreasing of the H_2O_2 reduction overpotential (~200 mV, estimated by the difference of cathodic peak potentials); (ii) a good electrocatalytic efficiency (ratio of $((I_{peak})_{[H2O2] = 5\ mM} - (I_{peak})_{[H2O2] = 0)}/(I_{peak})_{[H2O2] = 0}$), at an applied potential of −400 mV vs. $Ag/AgCl/KCl_{sat}$; 1.95. Overpotential decreases are advantageous, as this lowers the applied potential for further amperometric measurements to very close to 0 mV vs. $Ag/AgCl/KCl_{sat}$. The obtained electrodes present good electrocatalytic efficiency and suggest again that they are improved by the presence of the copper that was introduced into the zeolite sample [52]. These characteristics prove the the newly prepared electrodes can be used as efficient amperometric sensors for H_2O_2 detection.

Once the voltammetric electrocatalytic characterization of the newly obtained modified electrodes was completed, measurements with rotating disk electrodes were realized at different supporting electrolyte pH values, in 0.1 M phosphate buffer containing 20 mM H_2O_2 at a rotation speed of 800 rpm, to estimate the electroanalytic parameters of the elec-

trocatalytic reduction of H_2O_2. Thus, the optimum applied potential was determined from the dependence of the H_2O_2 electrocatalytic current on the applied potential (Figure 9A–C).

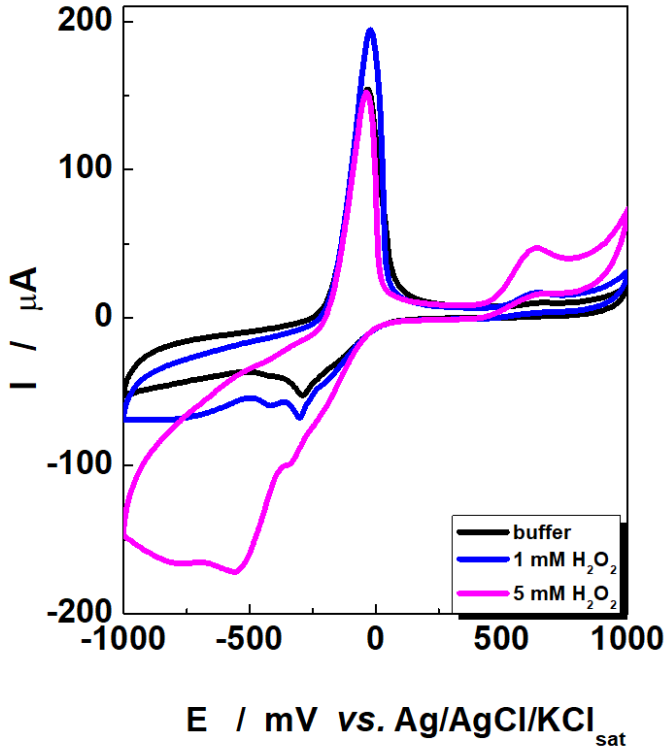

Figure 8. Cyclic voltammograms recorded with Cu–Z–CPE electrodes in 0.1 M phosphate buffer (pH 7.0) and in solution containing two H_2O_2 concentrations.

As can be seen in Figure 9A–C, the optimum value of applied potential was −50 mV vs. $Ag/AgCl/KCl_{sat}$ for pH 3, −150 mV vs. $Ag/AgCl/KCl_{sat}$ for pH 7 and −400 mV vs. $Ag/AgCl/KCl_{sat}$ for pH 9. For pH 3, the optimum value of applied potential was chosen as the higher value, while for pH 7 and pH 9, the optimum values were chosen on the plateau of the graph, because after this plateau, the values of the H_2O_2 electrocatalytic currents dramatically decreased. All these values were used in further electroanalytical measurements.

Figure 10 presents the calibration curves obtained from the amperometric measurements recorded in Figure S2, for the new modified electrodes Cu–Z-CPEs in 0.1 M phosphate buffer solutions with different pH values (3, 7 and 9), at increased values of H_2O_2 concentrations (between 10^{-5} to 10^{-1} M H_2O_2), rotation speeds of 800 rpm and using the values of applied potential determined above: −50 mV vs. $Ag/AgCl/KCl_{sat}$ (pH 3), −150 mV vs. $Ag/AgCl/KCl_{sat}$ (pH 7) and −400 mV vs. $Ag/AgCl/KCl_{sat}$ (pH 9).

The electroanalytical parameters were obtained from Figures 10 and S2 and are presented in Table 3. The sensitivity (calculated as the ratio of I_{max}/K_M, mA M^{-1}, according to Michaelis–Menten treatment [60]) was 0.75 (pH 3) < 0.87 (pH 7) < 27.8 (pH 9); in almost all cases, the linear domain reached up to 1 mM; the detection limit (calculated as a ratio of signal/noise of 3) was 10 µM (pH 3 and pH 7) and 31 µM (pH 9); in all cases, the response time was less than 1 min. Even at pH 9, the sensitivity was high and the applied potential was very low. The electroanalytical parameters determined at pH 7 are of interests due to the applied potential being close to 0 mV vs. $Ag/AgCl/KCl_{sat}$ and due to the possibility of the sensor for use in the detection of many analytes in environmental, food and medical applications in neutral pH media. The detection limit is better compared with other results already published for H_2O_2 sensors based on electrodes modified with zeolites [61–63] and are comparable with other H_2O_2 sensors based on carbon paste [64–66].

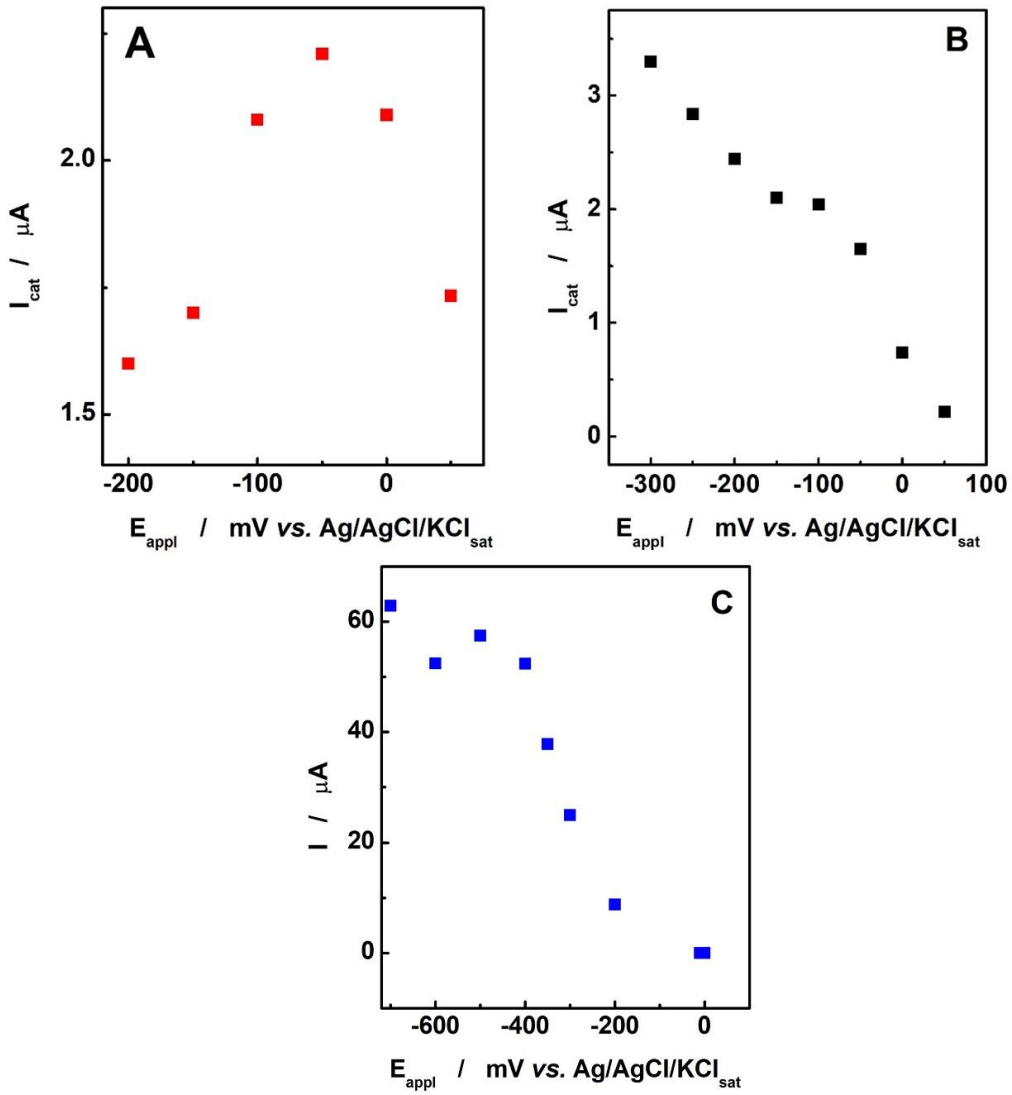

Figure 9. The influence of the applied potential on the H_2O_2 electrocatalytic current, recorded with Cu–Z–CPEs electrodes at different pHs of supporting electrolyte of pH 3.0 (**A**), pH 7.0 (**B**) and pH 9.0 (**C**).

Table 3. Electroanalytical parameters corresponding to Cu–Z-CPEs. Experimental conditions as in Figure 10.

pH	E_{appl} (mV)	Detection Limit (µM)	Linear Domain (M)	S (mA/M)	Chi^2	R^2
3	−50	10	10^{-5}–$5{\cdot}10^{-3}$	0.75	$1.8{\cdot}10^{-13}$	0.989
7	−150	10	10^{-5}–$3{\cdot}10^{-2}$	0.87	$4.1{\cdot}10^{-14}$	0.999
9	−400	31	$2{\cdot}10^{-5}$–10^{-3}	27.8	$1.0{\cdot}10^{-11}$	0.999

The durability of the H_2O_2 sensor was studied in different ways, to test their repeatability and reproducibility: (i) The voltammetric response of the modified electrode in the presence of 5 mM H_2O_2 over 100 cycles (Figure 11A) was tested, as well as the stability of the catalytic current of the modified electrode over 7 days (Figure 11B). In both cases, a decrease of less than 5% of the catalytic current was observed; (ii) Five modified electrodes were tested at the same H_2O_2 concentration (5 mM) and a small difference between signals occurred (5.4%; Figure 11C).

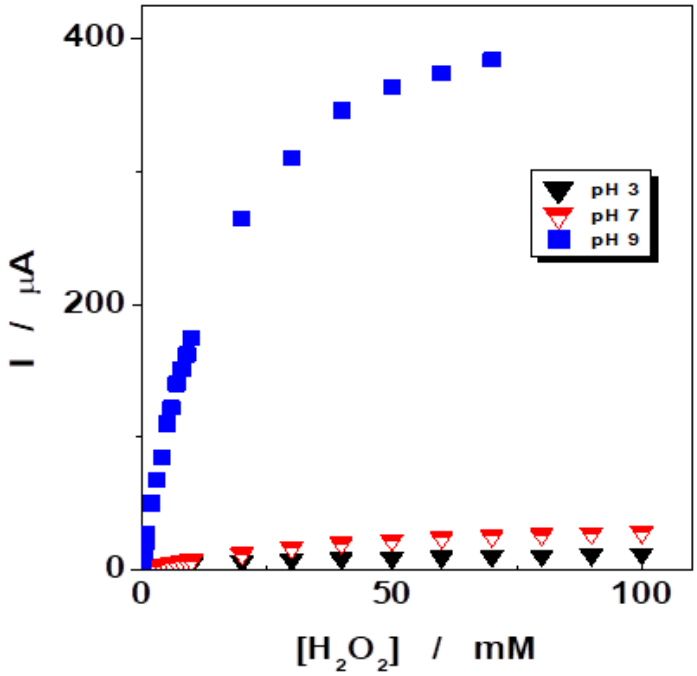

Figure 10. Calibration curves for H_2O_2 of Cu–Z-CPEs electrodes, at different pHs of phosphate buffer solution.

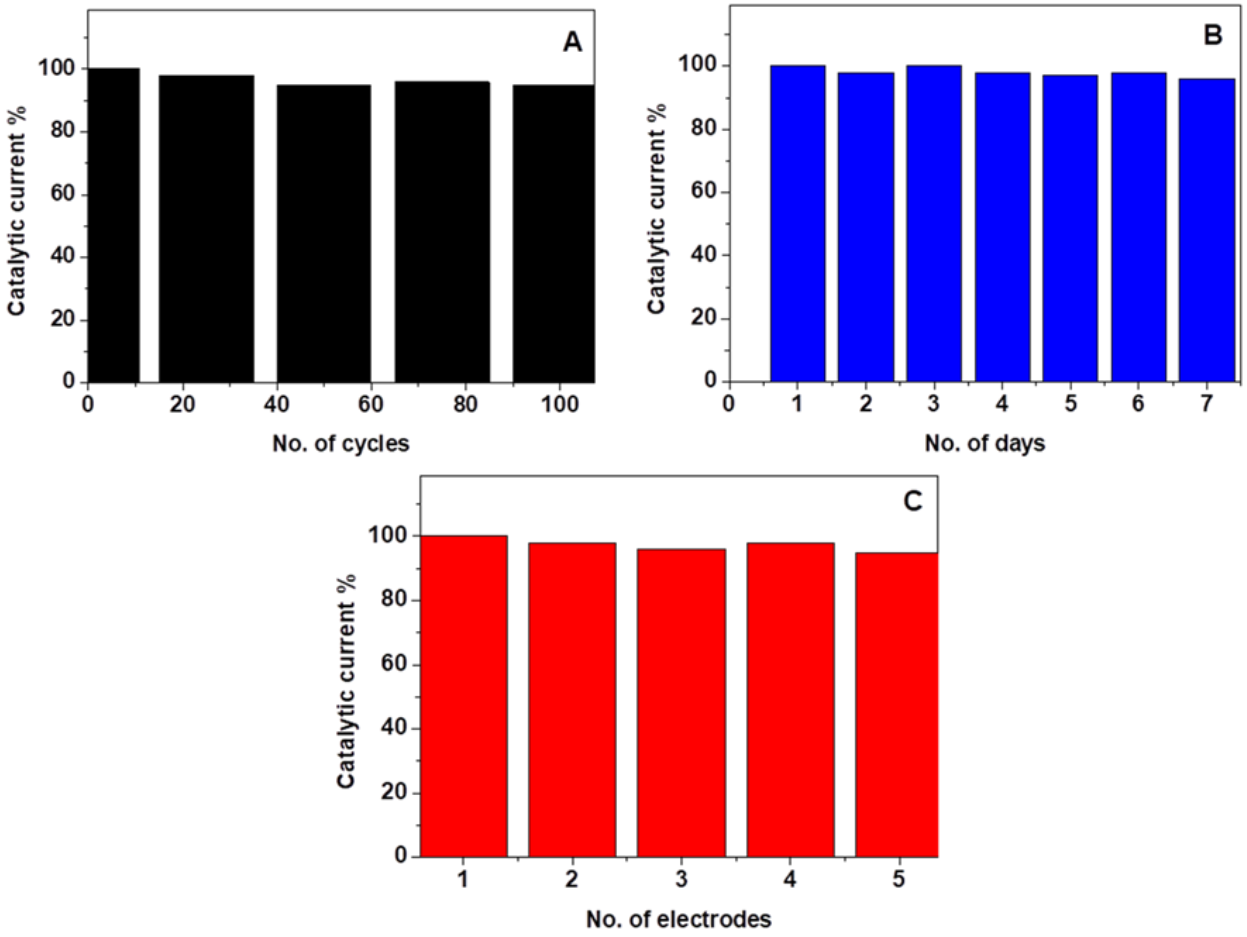

Figure 11. The durability of Cu–Z-CPEs sensor in the presence of 5 mM H_2O_2: repeatability over100 cycles (**A**) and 7 days (**B**); reproducibility of 5 electrodes (**C**).

4. Conclusions

Cu-exchanged zeolitic volcanic tuff was structurally and morphologically characterized using chemical analysis, energy dispersive X-ray spectroscopy, electron microscopy, X-ray diffraction spectroscopy and Fourier-transform infrared spectroscopy. A copper-exchanged zeolite-modified electrode was prepared by mixing copper–zeolite, graphite powder and paraffin oil to obtain new, low-cost amperometric sensors for H_2O_2 detection. Using cyclic voltammetry and amperometry techniques, the electrochemical reduction of hydrogen peroxide at the modified electrodes was investigated. The influence of pH and scan rate on the voltammetric response, characteristic of the modified electrodes, was studied and the optimum operating conditions were established. The new H_2O_2 amperometric sensor was electroanalytically characterized by the following parameters: a sensitivity of 0.87 mA/M, detection limit of 10 μM and linear domain up to 0.3 mM for H_2O_2 detection at pH 7, proving the possibility of its use for the detection of many analytes in environmental, food and medical applications.

Moreover, this natural material, which was used to obtain the H_2O_2 amperometric sensor—Cu-exchanged natural zeolite—is low-cost, decreases energy consumption and avoids pollution in many ways, over its whole life cycle. It is good for environmental applications due to the above-mentioned properties, and also for detecting different pollutants in various environmental media.

Supplementary Materials: The following supporting information can be downloaded at: https://www.mdpi.com/article/10.3390/chemosensors12020023/s1, Figure S1: Cyclic voltammograms corresponding to obtained Cu–Z-CPEs electrodes, recorded at increased scan rates of the electrode potential (between 5 mV/s and 320 mV/s), in 0.1 M phosphate buffer solution, pH 7, and Figure S2: The amperometric response of the modified electrodes Cu–Z-CPEs in 0.1 M phosphate buffer solutions with different pH values pH 7.0 (A), pH 3.0 (B) and pH 9.0 (C), at increased values of H_2O_2 concentrations (between 10^{-5} and 10^{-1} M H_2O_2), a rotation speed of 800 rpm and using the values of applied potential determined above: −50 mV vs. Ag/AgCl/KClsat (pH 3), −150 mV vs. Ag/AgCl/KClsat (pH 7) and −400 mV vs. Ag/AgCl/KClsat (pH 9).

Author Contributions: Conceptualization, D.G. and C.V.; investigation, D.G., S.A.M. and C.V.; resources, D.G., S.A.M. and C.V.; data curation, S.A.M. and C.V.; writing—original draft preparation, D.G. and S.A.M.; writing—review and editing, D.G., S.A.M. and C.V.; project administration, C.V.; funding acquisition, C.V. All authors have read and agreed to the published version of the manuscript.

Funding: This work was supported by grants from the Ministry of Research, Innovation and Digitization, CNCS/CCCDI—UEFISCDI, projects number PN-III-P1-1.1-TE-2021-0358.

Institutional Review Board Statement: Not applicable.

Informed Consent Statement: Not applicable.

Data Availability Statement: The data presented in this study are available on request from the authors.

Conflicts of Interest: The authors declare no conflicts of interest. The funders had no role in the design of the study; in the collection, analyses, or interpretation of data; in the writing of the manuscript; or in the decision to publish the results.

References

1. Elsayed-Ali, O.H.; Abdel-Fattah, T.; Elsayed-Ali, H.E. Copper cation removal in an electrokinetic cell containing zeolite. *J. Hazard. Mater.* **2011**, *185*, 1550–1557. [CrossRef]
2. Maicaneanu, A.; Bedelean, H.; Stanca, M. *Zeoliti Naturali. Caracterizare si Aplicatii in Protectia Mediului*; Editura Presa Universitara Clujeana: Cluj-Napoca, Romania, 2008; pp. 21–40. ISBN 9789736106736.
3. Oliver-Tolentino, M.A.; Guzmán-Vargas, A.; Arce-Estrada, E.M.; Ramírez-Rosales, D.; Manzo-Robledo, A.; Lima, E. Understanding electrochemical stability of Cu^+ on zeolite modified electrode with Cu-ZSM5. *J. Electroanal. Chem.* **2013**, *692*, 31–39. [CrossRef]
4. He, P.; Wang, W.; Du, L.; Dong, F.; Deng, Y.; Zhang, T. Zeolite A functionalized with copper nanoparticles and graphene oxide for simultaneous electrochemical determination of dopamine and ascorbic acid. *Anal. Chim. Acta* **2012**, *739*, 25–30. [CrossRef]

5. dos Santos, M.P.; Rahim, A.; Fattori, N.; Kubota, L.T.; Gushikem, Y. Novel amperometric sensor based on mesoporous silica chemically modified with ensal copper complexes for selective and sensitive dopamine determination. *Sens. Actuators B Chem.* **2012**, *171–172*, 712–718. [CrossRef]
6. Rohani, T.; Taher, M.A. A new method for electrocatalytic oxidation of ascorbic acid at the Cu (II) zeolite-modified electrode. *Talanta* **2009**, *78*, 743–747. [CrossRef]
7. Parpot, P.; Teixeira, C.; Almeida, A.M.; Ribeiro, C.; Neves, I.C.; Fonseca, A.M. Redox properties of (1-(2-pyridylazo)-2-naphthol)copper(II) encapsulated in Y Zeolite. *Microporous Mesoporous Mater.* **2009**, *117*, 297–303. [CrossRef]
8. Walcarius, A. Factors affecting the analytical applications of zeolite modified electrodes: Indirect detection of nonelectroactive cations. *Anal. Chim. Acta* **1999**, *388*, 79–91. [CrossRef]
9. Holkar, C.R.; Jadhav, A.J.; Pinjari, D.V.; Mahamuni, N.M.; Pandit, A.B. A critical review on textile wastewater treatments: Possible approaches. *J. Environ. Manag.* **2016**, *182*, 351–366. [CrossRef]
10. Kopacz, W.; Okninski, A.; Kasztankiewicz, A.; Nowakowski, P.; Rarata, G.; Maksimowski, P. Hydrogen peroxide—A promising oxidizer for rocket propulsion and its application in solid rocket propellants. *Fire Phys. Chem.* **2022**, *2*, 56–66. [CrossRef]
11. Sies, H. Role of metabolic H_2O_2 generation: Redox signaling and oxidative stress. *J. Biol. Chem.* **2014**, *289*, 8735–8741. [CrossRef] [PubMed]
12. Mihailova, I.; Krasovska, M.; Sledevskis, E.; Gerbreders, V.; Mizers, V.; Ogurcovs, A. Assessment of oxidative stress by detection of H_2O_2 in Rye samples using a CuO- and Co_3O_4-nanostructure-based electrochemical sensor. *Chemosensors* **2023**, *11*, 532. [CrossRef]
13. Miyamoto, F.; Saeki, M.; Yoshizawa, T. Improved protocol for an oxygen electrode method for determining hydrogen peroxide in foods. *J. AOAC Int.* **1997**, *3*, 681–687. [CrossRef]
14. Shariati-Rad, M.; Narges, S.; Farzaneh, J. Determination of hydrogen sulfide and hydrogen peroxide in complex samples of milk and urine by spectroscopic standard addition data and chemometrics methods. *RSC Adv.* **2017**, *46*, 28626–28636. [CrossRef]
15. Cibati, A.; Gonzalez-Olmos, R.; Rodriguez-Mozaz, S.; Buttiglieri, G. Unravelling the performance of UV/H_2O_2 on the removal of pharmaceuticals in real industrial, hospital, grey and urban wastewaters. *Chemosphere* **2022**, *290*, 133315–133323. [CrossRef] [PubMed]
16. Liu, X.; Xu, Y.; Ma, X.; Li, G. A third-generation hydrogen peroxide biosensor fabricated with hemoglobin and Triton X-100. *Sens. Actuators B Chem.* **2005**, *106*, 284–288. [CrossRef]
17. Wulansarie, R.; Rozaq, M.; Bismo, S.; Dyah, W.; Rengg, P. Degradation of Congo Red dye in wastewater using ozonation method with H_2O_2 catalyst. *J. Ilmu Lingkung.* **2024**, *22*, 150–154. [CrossRef]
18. Xin, S.; Huo, S.; Zhang, C.; Ma, X.; Liu, W.; Xin, Y.; Gao, M. Coupling nitrogen/oxygen self-doped biomass porous carbon cathode catalyst with $CuFeO_2$/biochar particle catalyst for the heterogeneous visible-light driven photo-electro-Fenton degradation of tetracycline. *Appl. Catal. B-Environ.* **2022**, *305*, 121024–121040. [CrossRef]
19. Ito, Y.; Tonogai, Y.; Suzuki, H.; Ogawa, S.; Yokoyama, T.; Hashizume, T.; Santo, H.; Tanaka, K.I.; Nishigakki, K.; Iwaida, M. Improved 4-Aminoantipyrine Colorimetry for Detection of Residual Hydrogen Peroxide in Noodles, Fish Paste, Dried Fish, and Herring Roe. *J. Assoc. Off. Anal. Chem.* **1981**, *64*, 1448–1452. [CrossRef]
20. Vinayagam, R.; Nagendran, V.; Goveas, L.C.; Narasimhan, M.K.; Varadavenkatesan, T.; Chandrasekar, N.; Selvaraj, R. Structural characterization of marine macroalgae derived silver nanoparticles and their colorimetric sensing of hydrogen peroxide. *Mater. Chem. Phys.* **2024**, *313*, 128787–128795. [CrossRef]
21. Monakhova, Y.B.; Diehl, W.K. Rapid 1H NMR determination of hydrogen peroxide in cosmetic products and chemical reagents. *Anal. Methods* **2016**, *8*, 4632–4639. [CrossRef]
22. Lu, J.; Lau, C.; Morizono, M.; Ohta, K.; Kai, M. A chemiluminescence reaction between hydrogen peroxide and acetonitrile and its applications. *Anal. Chem.* **2001**, *73*, 5979–5983. [CrossRef]
23. Tahirovic, A.; Copra, A.; Omanovic-Miklicanin, E.; Kalcher, K. A chemiluminescence sensor for the determination of hydrogen peroxide. *Talanta* **2007**, *72*, 1378–1385. [CrossRef] [PubMed]
24. Klassen, N.V.; Marchington, D.; McGowan, H.C. H_2O_2 determination by the I3-method and by $KMnO_4$ titration. *Anal. Chem.* **1994**, *66*, 2921–2925. [CrossRef]
25. Rubio-Clemente, A.; Cardona, A.; Chica, E.; Peñuela, G.A. Sensitive Spectrophotometric Determination of Hydrogen Peroxide in Aqueous Samples from Advanced Oxidation Processes: Evaluation of Possible Interference. *Afinidad* **2017**, *LXXIV*, 579. Available online: https://raco.cat/index.php/afinidad/article/view/328470 (accessed on 4 December 2023).
26. Li, J.; Dasgupta, P.K.; Tarver, G.A. Pulsed excitation source multiplexed fluorometry for the simultaneous measurement of multiple analytes. Continuous measurement of atmospheric hydrogen peroxide and methyl hydroperoxide. *Anal. Chem.* **2003**, *75*, 1203–1210. [CrossRef] [PubMed]
27. Oh, W.K.; Jeong, Y.S.; Kim, S.; Jang, J. Fluorescent polymer nanoparticle for selective sensing of intracellular hydrogen peroxide. *ACS Nano* **2012**, *6*, 8516–8524. [CrossRef] [PubMed]
28. Geng, Y.; Wang, Z.; Zhou, J.; Zhu, M.; Liu, J.; James, T.D. Recent progress in the development of fluorescent probes for imaging pathological oxidative stress. *Chem. Soc. Rev.* **2023**, *52*, 3873–3926. [CrossRef] [PubMed]
29. Ye, S.; Hu, J.J.; Zhao, Q.A.; Yang, D. Fluorescent probes for in vitro and in vivo quantification of hydrogen peroxide. *Chem. Sci.* **2020**, *11*, 11989–11997. [CrossRef] [PubMed]
30. Sun, H.; Xu, Q.; Ren, M.; Kong, F. A biocompatible chitosan-based fluorescent polymer for efficient H_2O_2 detection in living cells and water samples. *Int. J. Biol. Macromol.* **2024**, *257*, 128760–128769. [CrossRef]

31. Li, H.; Wu, Y.; Xu, Z.; Wang, Y. In situ anchoring Cu nanoclusters on Cu-MOF: A new strategy for a combination of catalysis and fluorescence toward the detection of H_2O_2 and 2,4-DNP. *Chem. Eng. J.* **2024**, *479*, 147508–147517. [CrossRef]
32. Rajamanikandan, R.; Ilanchelian, M.; Ju, H. Highly selective uricase-based quantification of uric acid using hydrogen peroxide sensitive poly-(vinylpyrrolidone) templated copper nanoclusters as a fluorescence probe. *Chemosensors* **2023**, *11*, 268. [CrossRef]
33. Botero-Cadavid, J.F.; Brolo, A.G.; Wild, P.; Djilali, N. Detection of hydrogen peroxide using an optical fiber-based sensing probe. *Sens. Actuators B Chem.* **2013**, *185*, 166–173. [CrossRef]
34. Tarvin, M.; McCord, B.; Mount, K.; Sherlach, K.; Miller, M.L. Optimization of two methods for the analysis of hydrogen peroxide: High performance liquid chromatography with fluorescence detection and high performance liquid chromatography with electrochemical detection in direct current mode. *J. Chromatogr. A* **2010**, *1217*, 7564–7572. [CrossRef] [PubMed]
35. Zhang, Y. An amperometric hydrogen peroxide sensor based on reduced graphene oxide/carbon nanotubes/Pt NPs modified glassy carbon electrode. *Int. J. Electrochem. Sci.* **2020**, *15*, 8771–8785. [CrossRef]
36. Zhou, C.; Cheng, R.; Liu, B.; Fang, Y.; Nan, K.; Wu, W.; Xu, Y. Cascade selective recognition of H_2O_2 and ascorbic acid in living cells using carbon-based nanozymes with peroxidase-like activity. *Sens. Actuators B Chem.* **2024**, *402*, 135118–135128. [CrossRef]
37. Wang, G.; Liu, J.; Dong, H.; Geng, L.; Sun, J.; Liu, J.; Dong, J.; Guo, Y.; Sun, X. A dual-mode biosensor featuring single-atom Fe nanozyme for multi-pesticide detection in vegetables. *Food Chem.* **2024**, *437*, 137882–137893. [CrossRef] [PubMed]
38. Yang, Z.; Tian, Z.; Zhang, X.; Qi, C. A novel strategy for realizing highly sensitive nonenzymatic detection of H_2O_2 based on regulating crystallinity of CoO nanosheets. *Microchem. J.* **2023**, *195*, 109540–109547. [CrossRef]
39. Ates, A.; Oskay, K.O. Evaluation of iron containing biochar composites prepared by different preparation methods for H_2O_2 sensing. *J. Taiwan Inst. Chem. E* **2023**, *152*, 105180–105195. [CrossRef]
40. He, Z.; Jin, Y.; Yuan, X.; Xue, K.; Hu, J.; Xiong, X. ZIF in situ transformation hollow porous self-supporting CoZn-LDH@CuO electrode for electrochemical sensing of glucose and H_2O_2. *Microchem. J.* **2023**, *195*, 109457–109467. [CrossRef]
41. Ahsan, M.; Dutta, A.; Akermi, M.; Alam, M.M.; Nizam Uddin, S.M.; Khatun, N.; Hasnat, M.A. Sulfur adlayer on gold surface for attaining H_2O_2 reduction in alkaline medium: Catalysis, kinetics, and sensing activities. *J. Electroanal. Chem.* **2023**, *934*, 117281–117290. [CrossRef]
42. Zhang, A.; Liu, Y.; Wu, J.; Zhu, J.; Cheng, S.; Wang, Y.; Hao, Y.; Zeng, S. Electrocatalytic selectivity to H_2O_2 enabled by two-electron pathway on Cu-deficient Au@Cu_{2-x}S-CNTs electrocatalysts. *Chem. Eng. J.* **2023**, *454*, 140317–140329. [CrossRef]
43. Jiang, L.; Wang, H.; Rao, Z.; Zhu, J.; Li, G.; Huang, Q.; Wang, Z.; Liu, H. In situ electrochemical reductive construction of metal oxide/metal-organic framework heterojunction nanoarrays for hydrogen peroxide sensing. *J. Colloid Interface Sci.* **2022**, *622*, 871–879. [CrossRef]
44. Han, J.; Kim, J.; Kim, B.-K.; Park, K. Hydrogel-based electrodeposition of copper nanoparticles for selective detection for hydrogen peroxide. *Chemosensors* **2023**, *11*, 384. [CrossRef]
45. Oliveira, M.R.F.; Herrasti, P.; Furtado, R.F.; Melo, A.M.A.; Alves, C.R. Polymeric composite including magnetite nanoparticles for hydrogen peroxide detection. *Chemosensors* **2023**, *11*, 323. [CrossRef]
46. Yang, Z.; Gao, Y.; Zuo, L.; Long, C.; Yang, C.; Zhang, X. Tailoring heteroatoms in conjugated microporous polymers for boosting oxygen electrochemical reduction to hydrogen peroxide. *ACS Catal.* **2023**, *13*, 4790–4798. [CrossRef]
47. Ma, X.; Tang, K.-L.; Lu, K.; Zhang, C.; Shi, W.; Zhao, W. Structural engineering of hollow microflower-like CuS@C hybrids as versatile electrochemical sensing platform for highly sensitive hydrogen peroxide and hydrazine detection. *ACS Appl. Mater. Interfaces* **2021**, *13*, 40942–40952. [CrossRef] [PubMed]
48. Li, Z.; Jiang, G.; Wang, Y.; Tan, M.; Cao, Y.; Tian, E.; Zhang, L.; Chen, X.; Zhao, M.; Jiang, Y.; et al. Detecting residual chemical disinfectant using an atomic Co–N_x–C anchored neuronal-like carbon catalyst modified amperometric sensor. *Environ. Sci. Nano* **2022**, *9*, 1759–1769. [CrossRef]
49. Bedelean, H.; Maicaneanu, A.; Burca, S.; Stanca, M. Investigations on some zeolitic volcanic tuffs from Cluj County (Romania), used for zinc ions removal from aqueous solution. *Stud. Univ. Babes-Bolyai Geol.* **2010**, *55*, 9–15. [CrossRef]
50. Maicaneanu, A.; Bedelean, H.; Burca, S.; Stanca, M. Evaluation of ammonium removal performances of some zeolitic volcanic tuffs from Transylvania, Romania. *Sep. Sci. Technol.* **2011**, *46*, 1621–1630. [CrossRef]
51. Rouquerol, E.; Rouquerol, J.; Sing, K. *Adsorption by Powders and Porous Solids. Principles, Methodology and Applications*; Academic Press: San Diego, CA, USA, 1999; pp. 18–20. [CrossRef]
52. Gligor, D.; Varodi, C.; Maicaneanu, A.; Muresan, L.M. Carbon Nanotubes-Graphite Paste Electrode Modified with Cu(II)-Exchanged Zeolite for H_2O_2 Detection. *Stud. Univ. Babsş-Bolyai Chem.* **2010**, *55*, 293–302. Available online: https://chem.ubbcluj.ro/~studiachemia/issues/chemia2006_2015/Chemia2010_2T2.pdf (accessed on 4 December 2023).
53. Bedelean, I.; Stoici, S. *Zeoliti*; Technical Publishing House: Bucharest, Romania, 1984; pp. 59–120.
54. Abreu, N.J.; Valdés, H.; Zaror, C.A.; Azzolina-Jury, F.; Meléndrez, M.F. Ethylene adsorption onto natural and transition metal modified Chilean zeolite: An operando DRIFTS approach. *Microporous Mesoporous Mater.* **2018**, *274*, 138–148. [CrossRef]
55. Ma, Y.-K.; Rigolet, S.; Michelin, L.; Paillaud, J.-L.; Mintova, S.; Khoerunnisa, F.; Daou, T.J.; Ng, E.-P. Facile and fast determination of Si/Al ratio of zeolites using FTIR spectroscopy technique. *Microporous Mesoporous Mater.* **2021**, *311*, 110683–110687. [CrossRef]
56. Inglezakis, V.J. The concept of "capacity" in zeolite ion-exchange systems. *J. Colloid Interface Sci.* **2005**, *281*, 68–79. [CrossRef] [PubMed]

57. Fanfan, P.N.; Mabon, N.; Thonart, P.; Lognay, G.; Copin, A.; Barthelemy, J.-P. Investigations on Cationic Exchange Capacity and Unused Bed Zone According to Operational Conditions in a Fixed bed Reactor for Water Lead Removal by a Natural Zeolite. *Biotechnol. Agron. Soc. Environ.* **2006**, *10*, 93–99. Available online: https://popups.uliege.be/1780-4507/index.php?id=1160 (accessed on 4 December 2023).
58. Bard, A.J.; Faulkner, L.R. *Electrochemical Methods: Fundamentals and Applications*, 2nd ed.; John Wiley & Sons, Inc.: Hoboken, NJ, USA, 2000.
59. Laviron, E. General expression of the linear potential sweep voltammogram in the case of diffusionless electrochemical systems. *J. Electroanal. Chem.* **1979**, *101*, 19–28. [CrossRef]
60. Makino, N.; Mochizuki, Y.; Bannai, S.; Sugit, Y. Kinetic Studies on the Removal of Extracellular Hydrogen Peroxide by Cultured Fibroblasts. *J. Biol. Chem.* **1994**, *269*, 1020–1025. Available online: https://pubmed.ncbi.nlm.nih.gov/8288557 (accessed on 4 December 2023). [CrossRef] [PubMed]
61. Maicaneanu, A.; Varodi, C.; Bedelean, H.; Gligor, D. Physical-chemical and electrochemical characterization of Fe-exchanged natural zeolite applied for obtaining of hydrogen peroxide amperometric sensors. *Chem. Erde Geochem.* **2014**, *74*, 653–660. [CrossRef]
62. Xue, F.; Qin, R.; Zhu, R.; Zhou, X. Sn species modified mesoporous zeolite TS-1 with oxygen vacancy for enzyme-free electrochemical H_2O_2 detecting. *Dalton Trans.* **2022**, *51*, 18169–18175. [CrossRef]
63. Muresan, L.M. Zeolite-modified electrodes with analytical applications. *Pure Appl. Chem.* **2011**, *83*, 325–343. [CrossRef]
64. Mosquera, N.; Aguirre, M.J.; Domingo, R.-L.; García, C.; Arce, R.; Bollo, S. Co_2SnO_4/carbon paste electrode as electrochemical sensor for hydrogen peroxide. *J. Chil. Chem. Soc.* **2017**, *62*, 3525–3528. [CrossRef]
65. Norouzi, B.; Malekan, A.; Moradian, M. Nickel-zeolite modified carbon paste electrode as electrochemical sensor for hydrogen peroxide. *Russ. J. Electrochem.* **2016**, *52*, 330–339. [CrossRef]
66. Rostami, S.; Azizi, S.N.; Ghasemi, S. Using of silver nanoparticles incorporated in nanoporous ZSM-5 hierarchical zeolite prepared from bagasse as a new sensor for electrocatalytic determination of H_2O_2 in biological samples. *J. Electroanal. Chem.* **2017**, *799*, 583–594. [CrossRef]